Temporal characterization of attosecond pulses emitted from solid-density plasmas

2010 New J. Phys. 12 043020

(http://iopscience.iop.org/1367-2630/12/4/043020)

New Journal of Physics
The open-access journal for physics

Temporal characterization of attosecond pulses emitted from solid-density plasmas

R Hörlein[1,2], Y Nomura[1,7], P Tzallas[3], S G Rykovanov[1,4], B Dromey[5], J Osterhoff[1], Zs Major[1,2], S Karsch[1,2], L Veisz[1], M Zepf[5], D Charalambidis[3,6], F Krausz[1,2] and G D Tsakiris[1,8]

[1] Max-Planck-Institut für Quantenoptik, Hans-Kopfermann-Strasse 1, D-85748 Garching, Germany
[2] Department für Physik der Ludwig-Maximilians-Universität München, Am Coulombwall 1, D-85748 Garching, Germany
[3] Foundation for Research and Technology-Hellas, Institute for Electronic Structure and Laser, PO Box 1527, GR-71110 Heraklion (Crete), Greece
[4] Moscow Engineering Physics Institute, Kashirskoe Shosse 31, 115409 Moscow, Russia
[5] Department of Physics and Astronomy, Queens University, Belfast BT7 1NN, UK
[6] Department of Physics, University of Crete, PO Box 2208, GR-71003 Voutes-Heraklion (Crete), Greece
E-mail: george.tsakiris@mpq.mpg.de

New Journal of Physics **12** (2010) 043020 (25pp)
Received 29 September 2009
Published 13 April 2010
Online at http://www.njp.org/
doi:10.1088/1367-2630/12/4/043020

Abstract. The generation of high harmonics from solid-density plasmas promises the production of attosecond (as) pulses orders of magnitude brighter than those from conventional rare gas sources. However, while spatial and spectral emission of surface harmonics has been characterized in detail in many experiments proof that the harmonic emission is indeed phase locked and thus bunched in as-pulses has only been delivered recently (Nomura *et al* 2009 *Nat. Phys.* **5** 124–8). In this paper, we discuss the experimental setup of our extreme ultraviolet (XUV) autocorrelation (AC) device in detail and show the first two-photon ionization and subsequent AC experiment using solid target harmonics. In addition, we describe a simple analytical model to estimate the chirp between

[7] Present address: Institute for Solid State Physics, University of Tokyo, Kashiwa, Chiba 277-8581, Japan.
[8] Author to whom any correspondence should be addressed.

the individual generated harmonics in the sub- and mildly relativistic regime and validate it using particle-in-cell (PIC) simulations. Finally, we propose several methods applicable to surface harmonics to extend the temporal pulse characterization to higher photon energies and for the reconstruction of the spectral phase between the individual harmonics. The experiments described in this paper prove unambiguously that harmonic emission from solid-density plasmas indeed occurs as a train of sub-femtosecond pulses and thus fulfills the most important property for a next-generation as-pulse source of unprecedented brightness.

Contents

1. Introduction

Rapid advances in laser technology have led to the production of ever shorter bursts of light allowing us to temporally resolve some of the fastest processes in atoms and molecules. This development has culminated in the generation of trains and even single extreme ultraviolet (XUV) pulses of attosecond (as) duration [1–3] from the interaction of moderately intense laser pulses with noble gases. Such pulses of attosecond duration have recently been used to study, for example, the ionization dynamics of noble gases in strong fields [4] or the emission of electrons from solid surfaces [5] in real time. While this method is very successful and has led to a whole series of ground-breaking discoveries it suffers from one fundamental limitation: owing to the fact that excessive ionization of the gas target has to be prevented in this generation process the driving laser intensity that can be used for harmonic generation is limited. Despite several attempts to improve the conversion efficiency [6–8], this imposes severe limitations on the maximum energy of the generated as-pulses. This renders XUV-pump–XUV-probe-type

experiments studying nonlinear processes, experiments addressing single-molecule imaging or the real-time observation of laser-plasma dynamics, impossible with such an XUV source [9].

To overcome this fundamental limitation, a different harmonic generation mechanism is required. The generation of high harmonics from the interaction of intense laser pulses with solid-density plasmas has been identified as a promising candidate that should allow the generation of as-pulses of unprecedented duration and intensity [10, 11]. The main advantage of this laser-plasma-based approach lies in the fact that it relies on the interaction of the incident laser field with the electron surface of a strongly ionized target and thus does not suffer from the limitation imposed on gas harmonics. On the contrary, the harmonic generation efficiency and the width of the generated harmonic spectrum increase strongly with increasing laser intensity, making this process highly scalable [11] and offering the potential for combining the high photon fluxes, currently only available at large-scale facilities like free-electron lasers, with the attosecond time resolution of laser-based sources.

Recent experimental and theoretical advances have identified two distinct mechanisms as sources of high harmonic radiation in the interaction of intense laser pulses with solid-density targets. At sub- and moderately relativistic intensities, coherent wake emission (CWE) [12–14] dominates while the relativistic oscillating mirror (ROM) mechanism becomes more efficient only for relativistic intensities, i.e. intensities resulting in a normalized vector potential $a_0 = |e|A_L/mc = \sqrt{I_L\lambda_L^2/(1.37\times10^{18}\,\mathrm{W\,cm^2\,\mu m^{-2}})} > 1$, and completely takes over in the relativistic limit ($a_0 \gg 1$) [10, 11, 15, 16]. The CWE process relies on Brunel electrons [17] injected into the pre-plasma gradient and the linear mode conversion of the plasma waves excited in their wake. As a result of this they exhibit a target density-dependent spectral cutoff that scales with the peak target density [18]. In contrast to that, in ROM, the harmonics are generated by the electrons in the plasma surface oscillating at relativistic velocities, resulting in a cutoff that is target independent and scales only with the laser intensity [19]. In addition, recent experiments have demonstrated that the harmonic emission from a solid target is beamed in the direction of the specular reflection under high-contrast conditions [18, 20, 21], have shown the transition from CWE to ROM harmonics [13, 18], addressed the issue of harmonic coherence [22] and have confirmed the theoretically predicted harmonic power-law scaling [23] and spectral cutoff [19] in the ultra-relativistic regime [11].

The most important characteristic to determine the usefulness of harmonics from solid surfaces as a source of intense as-pulses, however, has only been addressed very recently [24]. In this paper, we present in more detail the first measurement of the temporal structure of the harmonic emission in the CWE regime, which has proven for the first time that the harmonic emission from solid targets is indeed phase locked and capable of generating XUV pulses of sub-femtosecond (fs) duration. In addition to this, we present theoretical studies of the performance of our XUV-autocorrelator under realistic conditions and investigate the influence of density gradients in the target on the duration of the individual emitted as-pulses. Finally, we propose several ways in which our method for temporal characterization could be modified to study shorter (i.e. more energetic) as-pulses and allow the reconstruction of the spectral phase of the harmonics.

1.1. Attosecond pulse characterization techniques

Measuring the temporal structure of the harmonic emission from solid targets and other sources is one of the most challenging tasks in characterizing the properties of as-pulses. Independent

of the harmonic source, problems in conducting such experiments arise from the inherently low reflectivity of optics in the XUV spectral region and the fact that XUV radiation is strongly absorbed in bulk material, making the use of nonlinear crystals and conventional beam splitters impossible. Thus conventional techniques for temporal characterization used in the visible and near-infrared (IR) spectral region cannot be applied for XUV radiation. In addition, special problems in characterizing harmonics from solid surfaces arise from the limited number of shots that can be taken before changing the target and the large divergence of the emitted harmonic beam. Nevertheless, many studies have proposed and demonstrated methods to characterize the duration of XUV pulses synthesized from harmonics generated in gaseous media. The different methods can be divided into two main groups, the cross-correlation and nonlinear autocorrelation (AC) measurements. In addition, an extension of the spectral phase interferometry for the direct electric field reconstruction (SPIDER) method [25] to the XUV range has been proposed [26]. This method, however, requires the generation of harmonics from two different sources with slightly shifted central frequency and requires the additional assumption that the harmonic generation in these two sources is identical. We will restrict ourselves to methods capable of characterizing a single harmonic source in the following discussion.

The cross-correlation measurements rely on the superposition of the XUV pulse with an IR field and have been implemented in two schemes. The reconstruction of attosecond beating by interference of two-photon transitions (RABITT) technique [1] uses the fundamental electric field to produce sidebands in the photoelectron (PE) spectra generated with XUV photons. The average duration of the pulses within a train of as-pulses was inferred by observing the interference between the XUV and the IR pulse. Another technique called the attosecond streak camera [2, 27] uses the fundamental electric field to modulate the energy distribution of the PEs generated by the XUV photons. This modulation was used to determine the duration of the isolated as-pulses [2, 3, 28] and has subsequently also been applied to study attosecond dynamics in gases [4] as well as solids [5].

In contrast to cross-correlation methods, AC relies on the interaction of two replicas of the pulse to be characterized. The challenge of implementing AC measurements in the XUV lies in the fact that the experiments cannot be conducted using nonlinear crystals in the XUV. Instead, this is achieved by triggering two-photon ionization processes with the XUV radiation and subsequent detection of the generated ions or PEs. Several materials and different ionization processes have been investigated in this context such as two-photon ionization of helium [29, 30], two-photon above-threshold ionization (ATI) of helium [31–33], two-photon double ionization of helium [34] and two-photon ATI of argon [33, 35]. In all cases, the ions or PEs were detected using suitable ion or electron time-of-flight (TOF) spectrometers.

All the methods mentioned above have been demonstrated using harmonics generated from noble gases; their applicability to surface harmonics generated with 45 fs pulses, however, needs to be evaluated in detail to find the most promising method for our application. The duration of the driving laser pulses makes it necessary to use a method suitable of characterizing a train of as-pulses rather than a single pulse, which makes the use of an attosecond streak camera impossible in our case. The other cross-correlation method RABITT is meant to characterize a train of as-pulses; unfortunately it is not straightforward to apply RABITT to surface high harmonic generation (SHHG) however, as not only odd but also even harmonics are generated in the laser–solid interaction. These even harmonics will appear at the same position in the spectrum as the sidebands generated by the RABITT process, making it difficult to extract

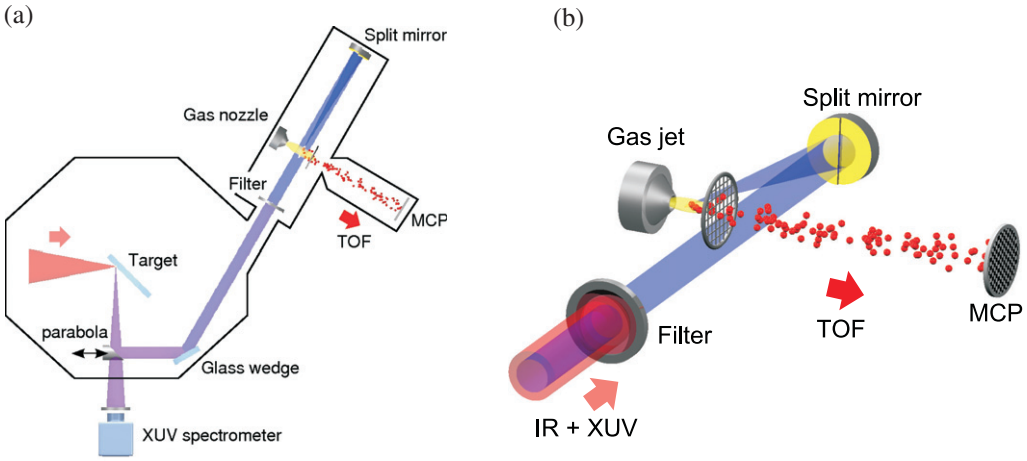

Figure 1. Schematic drawing of the experimental setup used for the AC measurement (a) and detailed view of the volume autocorrelator (b).

the necessary information from the PE spectra. In contrast to that, AC measurements using two-photon ionization processes are directly applicable to the SHHG process. In fact, the high XUV-pulse energy generated on each shot is actually beneficial in this case. The drawback of the AC technique, however, is that the usable photon energy range is strictly limited by the nonlinear medium, i.e. all photons that are energetic enough to ionize the target gas with a single photon need to be suppressed in the measurement. In other words, different media or different processes are needed to measure the duration of pulses in different wavelength regions.

From the above considerations, the volume AC using two-photon ionization of helium and the detection of the generated He^+ ions was chosen for our experiment. This technique certainly has a limitation in the applicable XUV photon energy; the required setup, however, is rather simple, consisting of a split mirror and a TOF setup, and the selection of the harmonic spectrum is readily possible by choosing the proper target and filter combination [18, 36]. The relatively simple and direct applicability to SHHG makes it suitable for the first attempt to characterize the temporal structure of harmonics generated from solid targets.

2. Experimental setup

The experiments presented in this work were conducted using the Ti:sapphire ATLAS laser facility at the Max-Planck Institute for Quantum Optics in Garching, Germany. The laser delivered 700 mJ pulses of 45 fs full-width at half-maximum (FWHM) in duration at 10 Hz repetition rate to the experimental chamber. The laser was focused to the target using an F/2.5 30° off-axis parabola (effective focal length $f_{\mathrm{eff}} = 168$ mm) resulting in a focus with a peak intensity of approximately 4×10^{19} W cm^{-2} and an average intensity over the area containing 86% of the total energy of 4×10^{18} W cm^{-2}. The 120 mm diameter disc targets were mounted on a mechanism allowing the acquisition of approximately 2500 shots at a repetition rate of up to 10 Hz and positioned under an angle of 45° to the incident p-polarized beam.

The beam transport and AC setup after the target are depicted in figure 1(a). The radiation generated on the target was re-collimated with a 1 inch gold-coated, 90° off-axis parabola with an effective focal length $f_{\mathrm{eff}} = 150$ mm and thus an F-number of 6. This allowed the collection

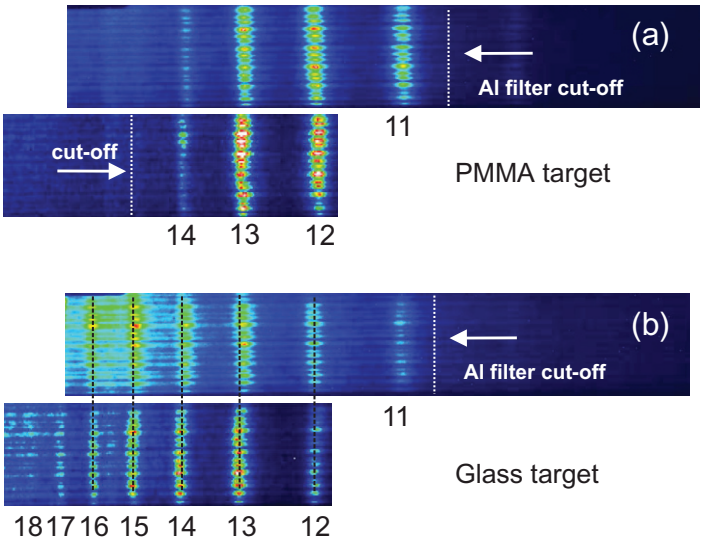

Figure 2. Typical harmonic spectra obtained using a 150 nm Al filter for (a) a low-density PMMA (density $\approx 1.2\,\mathrm{g\,cm^{-3}}$) and (b) a high-density glass target (density $\approx 2.7\,\mathrm{g\,cm^{-3}}$). The high-frequency cutoff (not shown in (b)) of the harmonic spectra is in good agreement with the predictions for harmonic generation via the CWE mechanism [12].

of a large fraction of the generated XUV radiation, which is emitted from the target with roughly half the divergence of the incident laser beam [18, 36]. The parabola was mounted on a flipper stage to allow the observation of the harmonic spectrum with a 1 m grazing incidence XUV spectrometer by moving the parabola out of the beam. Typical harmonic spectra recorded from different types of targets using a 150 nm Al filter in the spectrometer are shown in figure 2. The spectral cutoff observed for the low-density polymethylmethacrylate (PMMA) target is in good agreement with the cutoff predicted for harmonic generation via the CWE mechanism [12]. The beam collected with the parabola was reflected off a fused silica wedge at an angle of incidence (AOI) of approximately 57° close to the Brewsters angle for the p-polarized 800 nm fundamental of the laser to suppress residual IR radiation reflected from the target and prevent damage to the metallic filters positioned downstream. In the experiments presented here, a 150-nm-thick indium filter with a 1 inch clear aperture was used to limit the spectrum transmitted to the autocorrelator to the region between H8 and H16.

After spectral filtering the beam is focused into a pulsed gas jet using a split spherical mirror (focal length 150 mm) under a small angle (AOI 8°) whose one half can be delayed with respect to the other using a piezo-driven translation stage. Thus, the split mirror acts simultaneously as a beam splitter and as a delay stage in the AC, making other optics unnecessary. It has an unprotected gold coating to provide a nearly constant reflectivity of approximately 10% over the whole spectral range from H8 to H14. The ions generated in the focus of the XUV beam were accelerated with a static electric field into a TOF setup and time-resolved mass spectra were measured with an MCP and accumulated and averaged using a digital oscilloscope. A detailed sketch of the AC setup is shown in figure 1(b). Essentially, the setup of the AC used in this experiment is very similar to the one previously used for the AC of harmonics generated from noble gases [30, 37]; however, two important differences have to be noted. Firstly, the

gas nozzle is mounted in-line with the TOF in the new setup and floated at high voltage to act simultaneously as the repeller and prevent the problems of an extra metallic nozzle protruding into the accelerating field and distorting it and, secondly, the diameter of the XUV beam has been significantly increased, resulting in larger aberrations in the focus of the split mirror. The influence of this effect on the performance of the AC setup will be discussed in more detail in section 4.1 of this paper.

3. Two-photon ionization

Before an AC measurement can be conducted with confidence, it is of utmost importance to confirm that the ionization in the gas jet is indeed dominated by the two-photon process and is thus suitable for the second-order AC. In a first step, it is therefore necessary to verify that the focused intensity in the interaction region is high enough to generate enough ions through two-photon ionization. In order to estimate the XUV intensity (I_{XUV}) needed to observe a nonlinear process in atoms, the two-XUV-photon non-resonant ionization yield (Y_2) has to be calculated in realistic experimental conditions. For an XUV pulse of duration τ_{XUV} and intensity I_{XUV}, the transition probability rate (W_2) and the ion yield (Y_2) per pulse for a two-photon absorption process are given by

$$W_2 = \sigma^{(2)} \left(\frac{I_{\mathrm{XUV}}}{\hbar\omega} \right)^2 \text{ and } Y_2 = \sigma^{(2)} \left(\frac{I_{\mathrm{XUV}}}{\hbar\omega} \right)^2 \tau_{\mathrm{XUV}} N, \tag{1}$$

respectively, with N being the number of atoms in the interaction region. The number of ions (N_{ion}) generated is given by

$$N_{\mathrm{ion}} = n_{\mathrm{a}} V \sigma^{(2)} \int_{-\infty}^{\infty} \left(\frac{I_{\mathrm{XUV}}}{\hbar\omega} \right)^2 \mathrm{d}t \tag{2}$$

with n_{a} being the atomic density in the interaction volume V and $\sigma^{(2)}$ the generalized two-photon cross-section with values ranging from 10^{-49} to $10^{-52}\,\mathrm{cm}^4$ s. For realistic atomic densities (e.g. $n_{\mathrm{a}} = 10^{15}$–$10^{16}\,\mathrm{atoms\,cm}^{-3}$) and interaction volume (e.g. $V = 10^{-9}\,\mathrm{cm}^3$) an observable two-photon ionization yield requires XUV intensities higher than $10^9\,\mathrm{W\,cm}^{-2}$. This condition is well fulfilled in our experiment where focused XUV intensities of the order of 0.5–$1.0 \times 10^{11}\,\mathrm{W\,cm}^{-2}$ are achieved [24].

To verify experimentally that we can indeed ionize He via a two-photon process, the dependence of the yield of various ion species has been recorded as a function of the XUV intensity. Since the XUV intensity is difficult to measure directly in parallel to the detection of the generated ions, we use the O_2^+ signal, which is known to be generated via single-photon ionization in the photon energy range used (ionization potential 12.1 eV [38]), as a measure of the XUV intensity. Figure 3 shows the result of this measurement for a low-density PMMA target (red) with a sharp CWE cutoff at harmonic 14 (H14) and a high-density fused silica target with a cutoff at H20 (blue) for different ions species. A very obvious difference is visible in the intensity dependence of the He^+ ion yield in the two cases. While the measurement with the PMMA target and thus the CWE cutoff at H14 (see figure 2) in the harmonic spectrum clearly displays an intensity dependence with a slope of close to 2 for He^+ in the log–log plot, indicating two-photon ionization, the high-density target results in a slope of approximately one, indicating that the residual 16th harmonic contained in the spectrum in this case is sufficient to dominate the ionization process, resulting in mainly single-photon ionization. The reason for

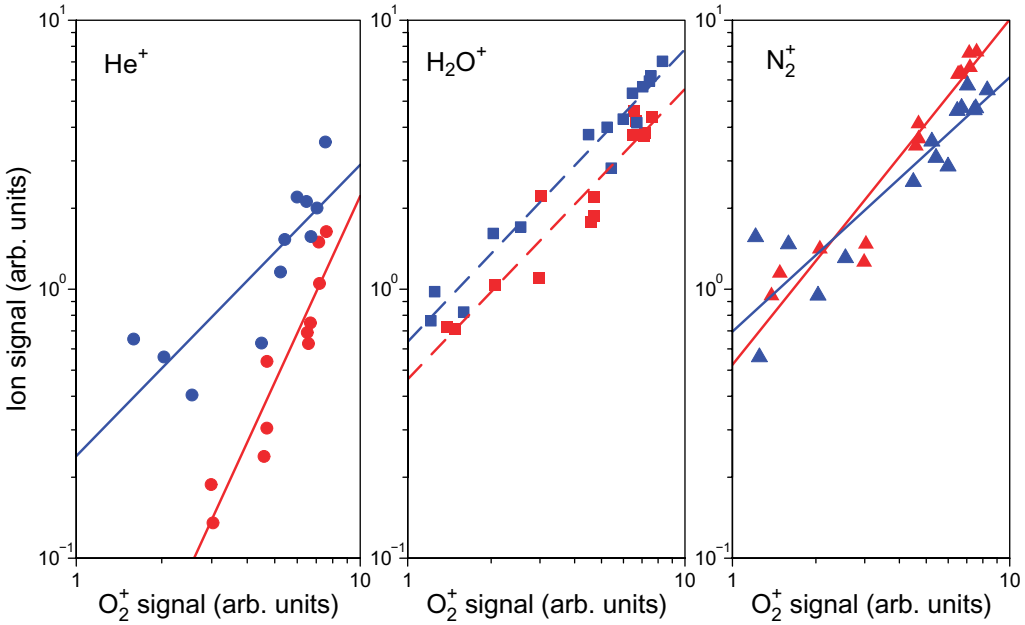

Figure 3. Ion yields of He^+, H_2O^+ and N_2^+ plotted as a function of the O_2^+ ion yield as measured in the TOF spectrometer for a low-density PMMA target (red) and a high-density fused silica target (blue). As the O_2^+ ions are generated via single-photon ionization for all harmonics selected by our filter [38], this is equivalent to plotting the ion yield versus XUV intensity. In this case, a slope of one indicates single-photon ionization, whereas a slope of two is evidence of a two-photon process. It is clearly visible that only in the case of the low-density target where harmonics above H15 are completely suppressed [24, 36], helium is ionized via a two-photon process.

this is illustrated in figure 4, where the harmonic spectrum from a PMMA target transmitted through an In filter is shown. It is obvious that it is mainly the property of the target that limits the harmonic spectrum to orders below 15 in this case and not the filter. A glass target will result in a significant number of higher energy photons in the interaction region of the AC. As the ionization yield for single-photon ionization of He is roughly five to six orders of magnitude higher than that for the two-photon process for the intensities used in the present experiment [39, 40], this will dominate the interaction in the case of a glass target. For comparison the intensity dependence of the ionization of two background gases is shown in figure 3. For both H_2O^+ and N_2^+, a slope of one indicating single-photon ionization is detected for both target materials as one would expect from the respective ionization potentials of 12.6 and 15.6 eV [38], which are both significantly lower than the energy of the highest harmonic in the spectral composition.

The measurements indicate how crucial proper spectral filtering, especially at the high-energy end of the harmonic composition used for the AC, is for the success of the experiment as only a two-photon process as a detector will allow the measurement of the XUV emission duration. For the measurements presented in the next section, we have therefore chosen a low-density PMMA target to take advantage of the spectral cutoff despite its less favorable material properties, especially its lower damage threshold, which leads to larger pre-plasma expansion

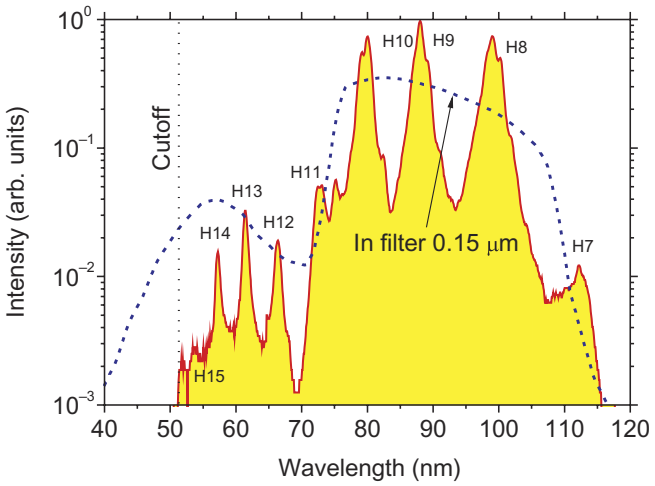

Harmonic	Relative amplitude
8	0.66
9	0.99
10	1.0
11	0.055
12	0.033
13	0.061
14	0.029

Figure 4. Harmonic spectrum from a low-density PMMA target after the transmission through a 150 nm In filter. The transmission curve of the filter is given for reference. Despite the relatively flat response of the filter between 50 and 70 nm, a clear cutoff originating from the PMMA target is observed in the spectrum. The table gives the relative intensities of the individual harmonics corrected for the reflectivity of the split mirror as the spectrum cannot be measured at this position.

and stronger target contamination and thus to a lower harmonic signal [36] as compared to the more robust fused silica targets.

4. The XUV AC

Having established the fact that the ionization of helium in our experiment is indeed the result of two-photon ionization, it is now possible to proceed with the volume AC of the XUV radiation. Before the results of the measurement are presented, however, it is illustrative to take a closer look at the special properties of the volume AC technique and especially investigate the influence of aberrations in the XUV focus introduced by the fact that the beam is reflected off the split mirror under a small angle in our experimental geometry (see figure 1). Following these considerations, the results of both the measurement of the XUV-emission envelope as well as the attosecond structure of the emitted radiation are presented.

4.1. The measurement method and the influence of aberrations on the AC signal

As has been mentioned above, we have chosen the method of volume AC [30, 37] to characterize the temporal structure of the XUV burst. Here we want to look at the properties of the AC trace in a little more detail as the volume AC technique is different from both the conventional interferometric as well as Michelson-interferometer-type intensity AC in two respects [37]. One is that the beam is split spatially into two replicas and changing the delay between them results in a spatial redistribution of the energy in the nonlinear medium. This is in contrast to the conventional amplitude-splitting arrangement, where the delay variation results in a change of the energy reaching the nonlinear crystal and the detector. The other difference is that as the

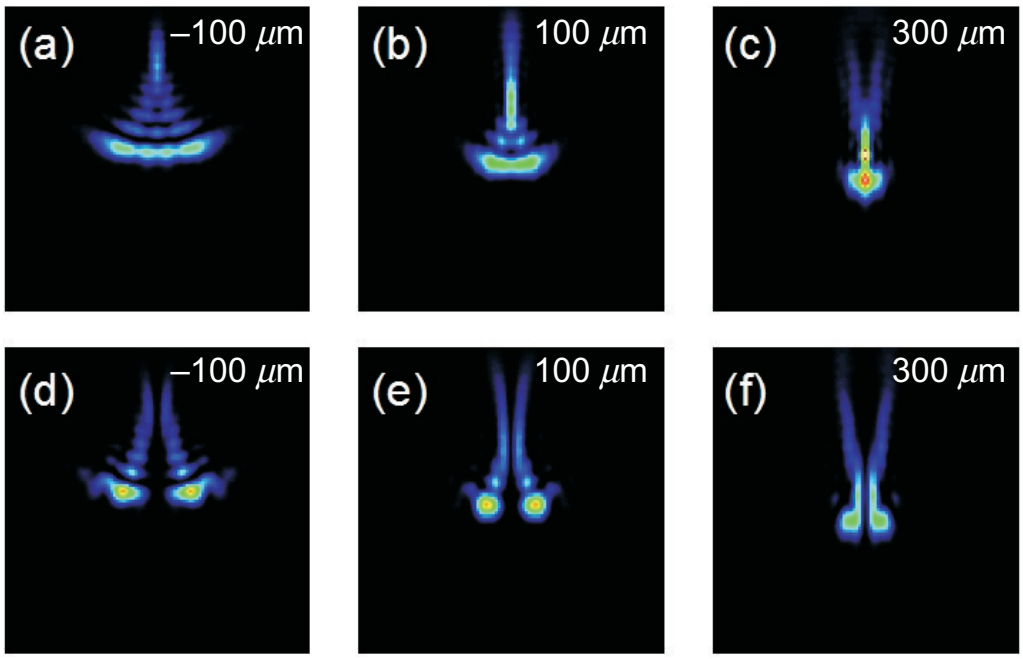

Figure 5. Simulated IR-intensity distributions at different points inside the focal volume. The position of each slice is given relative to the position of the nominal focus of the split mirror under normal irradiance. Panels (a)–(c) and (d)–(f) show intensity distributions for zero and half-cycle delay between the two halves of the split mirror, respectively.

delay variation is reflected in a varying spatial distribution of the energy in the focal volume, it is necessary to take into account the whole volume in which the interaction occurs, making it more complicated than when the amplitude-splitting method is used, where volume effects do not play a crucial role. These conceptual differences lead to a different signal-to-background ratio for both the interferometric and the intensity volume AC as compared to the conventional methods. Numerical simulations, taking into account the volume effect in the interferometric AC by calculating the intensity distribution at different positions in the propagation direction inside the focal volume, give a peak-to-background ratio of ∼2.75 : 1 for a second-order interferometric volume AC [37] as compared to the ratio of 8 : 1 obtainable with the conventional method. A similar effect is also found in intensity AC where the volume effects reduce the contrast ratio from 3 : 1 to 2 : 1. Nevertheless, despite this reduction in peak-to-background ratio, these results still show that volume AC can certainly be used to determine the temporal structure of the XUV emission.

In our experiment, an additional complication is introduced by the rather large tilt angle of ∼8° between the incoming and the reflected beams necessary to position the plume of the gas jet outside the 25 mm diameter incident XUV beam. This will introduce aberrations in the intensity distribution in the focal volume, which have been observed experimentally [41] and which are not negligible and which might decrease the signal-to-background ratio compared to the ones obtained in earlier work [37, 42].

To address this issue, we have conducted numerical simulations similar to the ones shown in [37] but including the off-axis focusing geometry and thus the effects of the aberrations. To demonstrate this, figure 5 shows the resulting intensity distributions of the IR beam at

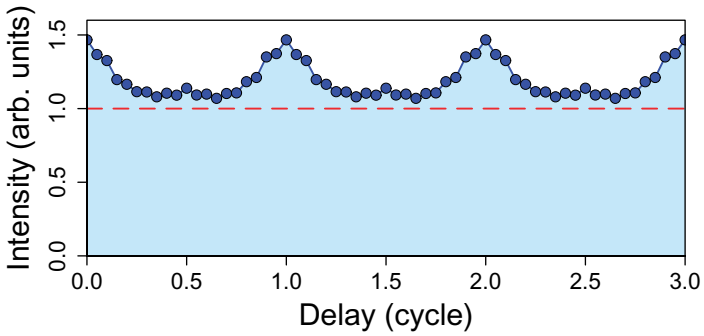

Figure 6. AC trace obtained from simulation. A periodic structure of sub-cycle pulses constituting a train is clearly observable. The horizontal dashed line shows the background level. The peak-to-background ratio is approximately 1.5 : 1.

different positions inside the focal volume. The simulated intensity distributions clearly display signatures of the astigmatism introduced by the off-axis focusing like the line-shaped structure best visible in figure 5(a), but the splitting of the focus into two structures characteristic for the introduction of a delay of one half cycle [37] in the focus is still clearly visible despite this. Therefore, the volume AC should still provide a sufficient signal-to-background ratio to measure the duration of the individual XUV pulses.

To evaluate this in detail for our experimental geometry, we have conducted the same simulation shown in figure 5 for three equally intense harmonics (H8 to H10) with a flat relative phase, corresponding to the main harmonics transmitted through the indium filter used for spectral selection. In the simulations, only three harmonics were considered in order to keep the necessary computation time at a reasonable level. For the sake of simplicity the amplitude of the pulse train was assumed to be constant over time, i.e. the simulation included no information about the envelope of the pulse train. The focal volume used for the full scan was $15\,\mu\text{m} \times 50\,\mu\text{m} \times 150\,\mu\text{m}$. Figure 6 shows the intensity AC trace obtained from the simulation in which one distinct peak with sub-cycle duration is observed for each laser cycle. Note that this is different from the case of gas harmonics where two pulses per cycle are observed corresponding to the fact that the harmonic spectrum in that case contains only odd harmonic orders [37]. Since no envelope was included in the simulation, the background level was obtained separately by simulating only half of the beam so that no interference occurs, and then multiplying the obtained value by 2, which is equivalent to setting the delay $\Delta\tau \to \infty$. The peak-to-background ratio is found to be approximately 1.5 : 1. This value is lower compared to the values obtained in other works [37, 42] as a result of the aberrations in the XUV focus. Nevertheless, this simulation shows that the modulations should still be observable in our experimental geometry.

4.2. The coarse scan

Provided that the generation process of the helium ions is second order, AC traces can be measured by observing the evolution of the helium ion signal as a function of the delay between the two parts of the beam reflected off the two halves of the split mirror. On the other hand, if the delay scan is conducted with a coarse step size such that this interference is not resolved, the under-sampling will cause aliasing and only the overall tendency of the AC trace

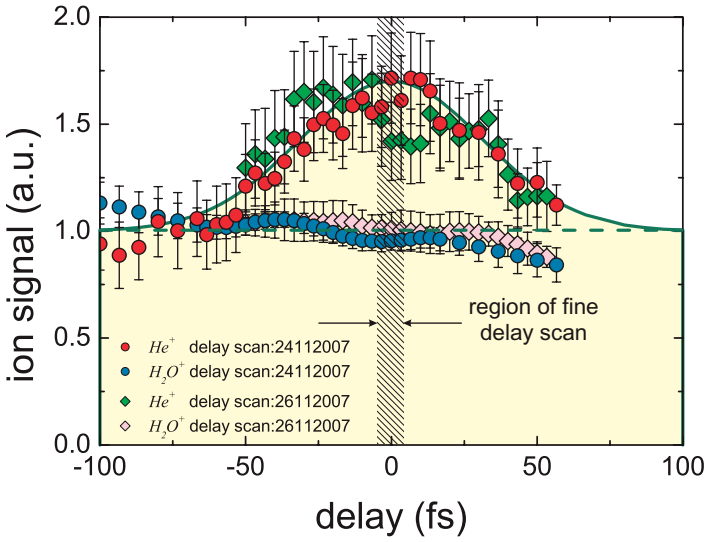

Figure 7. AC traces recorded on different days by measuring the dependence of the He^+ signal on the delay between the two XUV replica. The delay step size was 3.3 fs. The red circles and the green rhombus are the moving average of four points on each side, which reduces noise and makes the structure more clearly visible. The duration of the envelope of the XUV pulse train obtained from a fit to the raw data is in both cases ~ 44 fs. The H_2O^+ signal (blue circles) has been measured simultaneously with the He^+ signal (purple rhombus) and used as a reference. The traces show no significant peak compared to the background level, which is expected as the ionization process is linear in this case. The dashed area denotes the temporal window in which the fine scan presented in the next section was conducted.

will be observed. In other words, the measured coarse AC will reflect the shape of the envelope of the XUV pulse train [37], which corresponds to intensity AC in conventional terminology.

To measure a coarse AC trace, the evolution of the helium ion signal with delay was observed by varying the relative position of the two components of the split mirror in 0.5 μm steps, corresponding to 1 μm of light path difference and 3.3 fs of delay. This is larger than one cycle of the fundamental laser pulse and hence will not resolve the fine pulse structure within the XUV pulse train. For each delay, 20 laser shots were accumulated to measure one mass spectrum. The He^+ signals were obtained from the measured ion spectra and plotted against the delay. Figure 7 shows two such AC traces obtained on different days. To make the trend more obvious, the moving average over nine adjacent data points was taken for the correlation traces. The error bars indicate the standard error of the moving average. Instead, a clear peak structure is observed in the He^+ signal. For comparison we also plot the evolution of the H_2O^+ signal (blue dots and gray squares in figure 7) with delay, which we know to originate from single-photon ionization (see figure 3). In this trace, no signal dependence with delay is observed as one would expect, as the linear signal only depends on the total XUV energy in the interaction volume, which stays constant during the delay scan.

To deduce the duration of the overall XUV burst, we used a Gaussian fit to the raw data. We chose to fit the raw data instead of the moving average, as taking the moving average is

equivalent to a signal convolution with a rectangular window function, i.e. it broadens the width of the burst. Despite the large fluctuation of the raw data, the fitted curve nicely lies on the points deduced from the moving average. The width of the AC is obtained as (62 ± 28) fs, corresponding to a duration of the envelope of the XUV pulse train of (44 ± 20) fs, as the width of the AC trace is a factor of $\sqrt{2}$ larger than that of the measured pulse, when a Gaussian profile is assumed. All pulse durations are given as the FWHM in intensity unless otherwise noted. The rather large error is attributed to the large fluctuation of the raw data. From the fit it is also possible to extract the peak-to-background ratio of the AC trace, yielding a value of $(1.7 \pm 0.3) : 1$, which within the experimental error matches the ratio of $1.5 : 1$ obtained from the simulation shown in figure 6.

The effect of the adjacent averaging on the AC signal duration τ_0 can be estimated using the expression $\tau_0'^2 \approx \tau_0^2 + \tau_F^2$, which is strictly valid for the convolution of two Gaussians, where τ_F^2 is the width of the smoothing function and τ_0' the resulting width after smoothing. In our measurement, $\tau_0 \approx 62.2$ fs as deduced from the fit to the raw data and $\tau_F \approx 8 \times 3.3 = 26.4$ fs, resulting in a smoothed signal duration of $\tau_0' \approx 67.6$ fs. This represents less than 10% difference and, as a consequence, the fitted curve and the smoothed signal are almost indistinguishable.

It is interesting to note that the overall XUV emission duration of ~44 fs is almost the same as the incident near-IR driver pulse duration of ~45 fs. This implies that the CWE mechanism generating the harmonics in our case scales, unlike harmonic generation from noble gases, nearly linearly with the incident laser intensity. This finding is supported by earlier results [12, 22], which also report a near-linear dependence of the CWE harmonic signal on laser intensity.

4.3. The fine scan

To observe the expected as-pulse train in the AC trace, the relative delay introduced by the split mirror must be chosen small enough so that the resulting fringe structure can be resolved. In our experiment, the ion spectra were measured by scanning the split mirror in steps of 20 nm over a total distance of ~1.5 μm. As the effective path length difference corresponds to twice this value, this results in a scan over a time window of ~10 fs with a resolution of ~0.13 fs per step. This step size means that there are 20 data points in every laser cycle, which should be enough to resolve the fine structure, i.e. the as-pulse train, within the harmonic emission. At each position, a mass spectrum is obtained by accumulating the signal from 20 laser shots. From these raw ion spectra, the He^+ signals are extracted and plotted as a function of the relative delay. Since the fluctuations are rather large and it is difficult to see the tendency, we again use the moving average over nine points (four points from each side), i.e. we processed the data in the same way as we did in the analysis made in the previous section to visualize the trend more clearly. The resulting traces for two fine scans are shown as red squares with the error bars indicating the standard error of the moving average in figure 8.

From the AC traces, one can clearly see that there is a periodic structure with a separation of one laser cycle between the individual pulses in the train. To analyze this structure quantitatively, we fit successive Gaussian pulses with a background to the raw AC trace data. For the fit we make the assumption that the separation between the individual pulses is fixed to the duration of one laser period 2.67 fs. The other parameters such as the amplitude of each peak, the background level and the width of the pulses were left free. The width of the individual Gaussian pulses in the train deduced from the fit was found to be (1300 ± 500) as. From this value, the

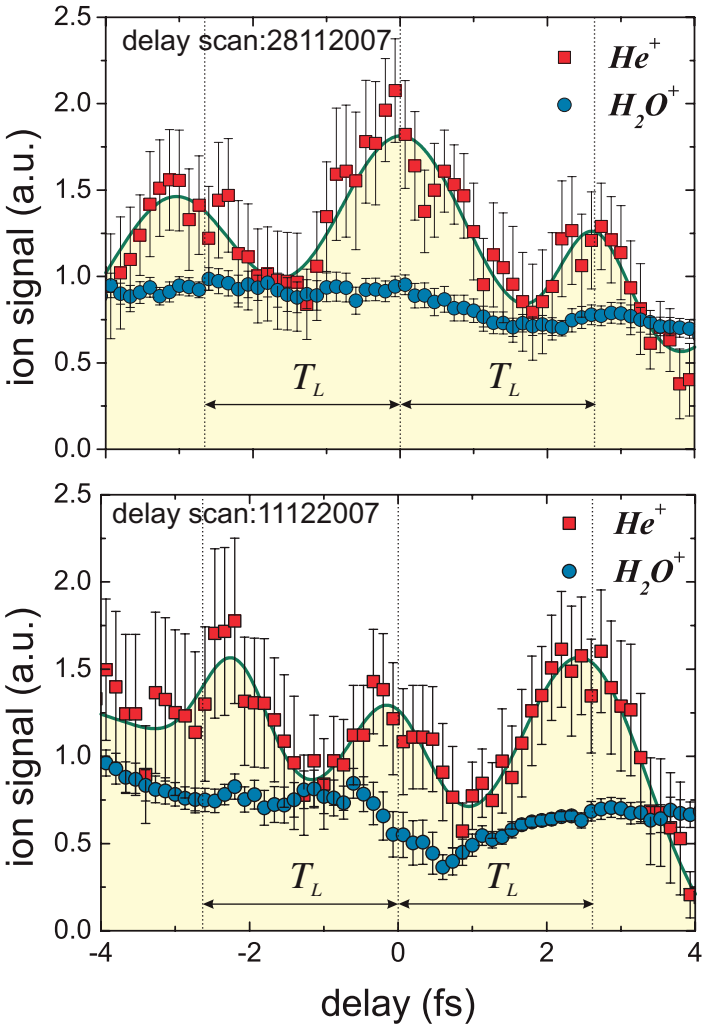

Figure 8. Fine AC traces recorded on different days by measuring the dependence of the He^+ signal on the delay between the two XUV replicas. The delay step size was 0.13 fs. Red squares show the moving average of the raw data, taking four points from each side. Several peaks are observed with the periodicity of T_L. The green curve is a fit to the smoothed data and is a guide to the eye. The vertical lines are placed with the same period to divide the trace into the individual driving laser cycles and visualize the periodic structure. The H_2O^+ signal (blue dots) has been measured simultaneously with the He^+ signal and used as a reference. No significant modulation is observed in this case. The lower signal at the end of the trace is attributed to a slight degradation in the XUV intensity.

duration of the individual pulses within the XUV train is obtained to be (900 ± 400) as, i.e. it is considerably shorter than the period of the driving laser and thus a clear indication of as-bunching in the harmonic emission. Note that using the deconvolution factor for a Gaussian pulse is only an approximation as the exact shape of the as-pulses is unknown. The variation

in the contrast of the individual pulses in the train during the scan is most probably the result of fluctuations in the XUV intensity during the measurement. This is also supported by the simultaneous variations observed in the single-photon signal of H_2O^+ (blue dots in figure 8), indicating a decrease of the overall XUV energy in the interaction region in the course of the scan.

To interpret this result, it is instructive to calculate the Fourier-limited duration of the individual as-pulses expected in our experiment. For this purpose, we have determined the relative amplitude of the individual harmonics in the composition by taking the convolution of the harmonic spectrum measured through a 150 nm In filter with the theoretical values for the reflectivity of the fused silica wedge and the split mirror. For reference these values are also given in the table in figure 4. Fourier transforming this spectrum assuming a flat phase yields a duration of each individual as-pulse of ~500 as, significantly shorter than the measured value. Owing to the fact that the uncertainty in our measurement is very large, it is not possible to prove that the observed discrepancy between the measured pulse duration and the Fourier-limited one is the result of a non-flat phase; nevertheless such a temporal broadening is actually expected for CWE as the individual harmonics are generated at different depths inside the pre-plasma density gradient, leading to a phase lag between them as a result of the different propagation distances to the plasma surface [12, 43].

5. Theoretical considerations

To study the influence of the pre-plasma gradient on the duration of the individual as-pulses in more detail theoretically, we have developed a simple analytical model to estimate the relative phase between the individual harmonics. In addition, a wavelet analysis [44, 45] of the results of one-dimensional particle-in-cell (PIC) simulations supports the assumptions made in the simple model and shows that it is indeed applicable to the complicated dynamics of the harmonic generation process. Both of these approaches shall be discussed in the following paragraphs.

5.1. Analytical approach

The analytical model of the phase delay between the individual harmonics is based on the idea that each individual harmonic q is generated at the point inside the pre-plasma gradient where the local plasma frequency is exactly $q\omega_0$. The model is also described in [43]. In the case of a linear density gradient of length L starting at the position $x = 0$, these positions $x(q)$ inside the density gradient are given by

$$x(q) = L\frac{n_c}{n_{max}}q^2, \tag{3}$$

where n_c and n_{max} denote the critical and the maximum target density, respectively. Considering that the total phase delay between the individual harmonics is the result of both the different distance the electrons need to travel until they excite the respective harmonic and the propagation of the XUV radiation out of the gradient and allowing for oblique incidence of the driving laser, the relative phase between the individual harmonics $\phi(q)$ is given by

$$\phi(q) = 2\pi\frac{L}{\lambda_L}\frac{n_c}{n_{max}}q^3\left[\frac{c}{v_e\cos(\Theta_{in,e})} + \frac{c}{v_{ph}\cos(\Theta_{out,ph})}\right], \tag{4}$$

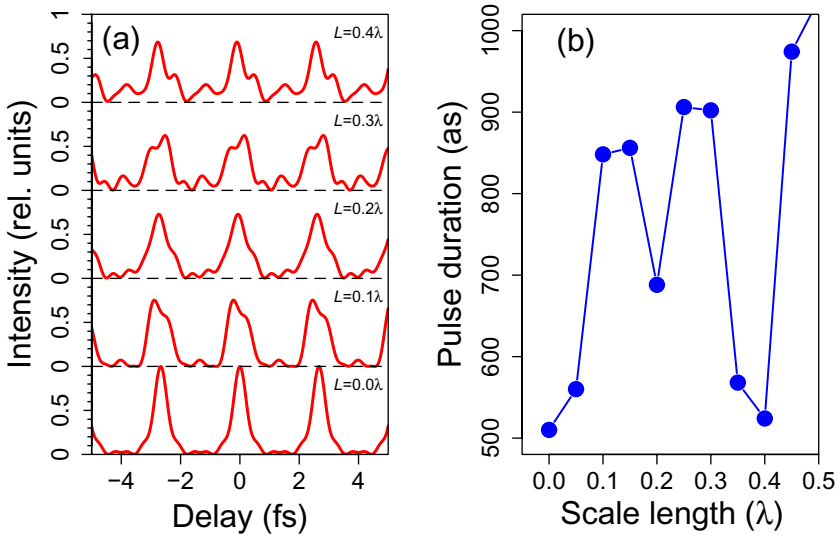

Figure 9. Influence of different scale lengths pre-plasmas on the generated as-pulse train. (a) Envelopes of pulse trains synthesized using the harmonic spectrum in the gas jet of the volume autocorrelator and different values of the pre-plasma scale length. The relative phases between the harmonics were calculated using equation (4) and assuming $\Theta_{\mathrm{in,e}} = \Theta_{\mathrm{out,ph}} = 45^\circ$ and $v_\mathrm{e} = c$. In (b), the FWHM duration of the main pulses in the as-pulse trains shown in (a) are plotted as a function of plasma scale length. The duration oscillates between 500 and 900 as for scale lengths shorter than 0.4λ. Note, however, that in the case of $L = 0.4\lambda$, considerable amounts of the pulse energy are scattered into the wings of the individual as-pulses and the determination of the pulse duration becomes difficult.

where c is the speed of light in the vacuum, λ_L the laser wavelength, v_e and v_ph the propagation velocity of the electrons and the generated photons inside the density gradient and $\Theta_{\mathrm{in,e}}$ and $\Theta_{\mathrm{out,ph}}$ the angle of the incident electrons and the outgoing photons with respect to the target normal.

To analyze the influence of such a chirp on the duration of the individual as-pulses in the pulse train generated in our experiment, we have conducted a Fourier-transform analysis of harmonic spectra similar to the ones present in the gas jet of our volume autocorrelator (calculated from the measured harmonic spectrum multiplied by the transmission curve of the In filter and the reflectivity of the fused silica wedge and the split mirror (see figure 1)) with chirps calculated from equation (4). To adapt the equation to our conditions, we chose $\Theta_{\mathrm{in,e}} = \Theta_{\mathrm{out,ph}} = 45^\circ$ and $n_\mathrm{max} = 200 n_\mathrm{c}$ and assumed $v_\mathrm{e} = c$ for the relativistic intensities achieved in our experiment. The resulting pulse trains calculated for different values of L and a plot of the as-pulse duration versus scale length are shown in figure 9. As the scale length is increased, the duration of the individual as-pulses increases quickly from the Fourier-limited 500 as to values around 900 as. It is important to note here that the value for the duration given for $L = 0\lambda$ is somewhat artificial as the generation of CWE harmonics always requires a small but nonzero pre-plasma [46, 47]. The value can, however, be understood as the pulse duration expected from the harmonics generated via the ROM mechanism as this is expected to generate harmonics

with a flat phase [11]. For very long scale lengths around $L = 0.4\lambda_L$, the duration briefly drops back down to around 500 as, before it becomes impossible to identify individual pulses for pre-plasmas of longer scale lengths. It should be noted, however, that for $L = 0.4\lambda_L$, a large fraction of the energy is already scattered into the wings of the as-pulses, making the FWHM-duration value somewhat misleading (see the top plot in figure 9(a)).

Despite the simplicity of the model and the large error in the measured value of the duration of the individual as-pulses, it is interesting to see that the model predicts pulse durations close to the measured one of 900 as for a whole range of pre-plasma gradients with scale length between 0.1 and $0.3\lambda_L$. In fact, agreement between the measurement and the calculation is much better when a short pre-plasma, which is certainly present in the experiment, is assumed than in the case $L = 0$. Owing to the insensitivity of the second-order AC measurement to the exact pulse shape of the emitted radiation and the limited accuracy of our measurement, this can certainly not be seen as a measurement of the density gradient scale length; it does however motivate the development of temporal characterization methods that are capable of measuring the relative phase between the harmonics as such a measurement can also be used to reconstruct the shape of the density gradient in the harmonic target. Possible methods for characterizing the phase of the emitted harmonics will be discussed in section 6 of this paper.

5.2. *Wavelet analysis*

To check whether the predictions of the simple model calculation actually hold true for the very complex dynamics in the vacuum plasma boundary, we have conducted a series of one-dimensional (1D) PIC simulations for targets with linear density ramps of various lengths and with parameters close to those in the experiment. For the simulation, we chose a peak target density of $n_{max} = 200n_c$ with a linear density gradient of length L, a pulse duration of $\tau_{FWHM} = 10$ cycles in the electric field and 45° AOI. The normalized vector potential was set to $a_0 = 0.2$ to suppress relativistic effects and simulate only the generation of harmonics via the CWE mechanism.

The wavelet or time–frequency analysis [44, 45] of the harmonics obtained from simulations for two different values of the pre-plasma scale length is shown in figure 10. A time delay between the emission of the lower and the higher harmonics within every cycle of the driving laser is clearly visible with lower order harmonics preceding the higher ones. In addition, the comparison of the two simulations also shows that the effect becomes more pronounced in the case of a longer pre-plasma. Both of these findings are in agreement with the physical picture on which the simple model presented above is based, namely the assumption that higher harmonics are generated deeper inside the target, causing them to arrive at the detector later than the lower orders. In the case of a longer gradient, this delay becomes larger, leading to a larger tilt angle in the time–frequency plot. In this context, it is also interesting to note that harmonics generated in the relativistic regime via the ROM mechanism do not display this behavior but are all emitted at the same time independent of the pre-plasma scale length [43].

To analyze the influence of the chirping of the individual emitted as-pulses on their duration and allow a more direct comparison of the simulations with the simple model, figure 10 also shows the as-pulse train synthesized from harmonics 8–10 under the respective conditions (yellow curves in figures 10(a) and (b)). H8–H10 were chosen from the simulated spectrum as

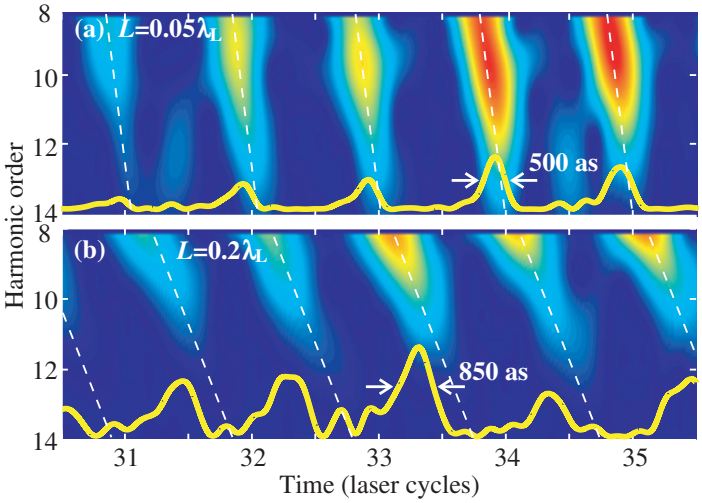

Figure 10. Wavelet (time–frequency) analysis of 1D–PIC simulation results of the harmonic emission from a target with linear density gradient of (a) $L = 0.05\lambda_L$ and (b) $L = 0.2\lambda_L$. The simulation parameters were chosen as $n_{max} = 200n_c$, $a_0 = 0.2$, a pulse duration of $\tau_{FWHM} = 10$ cycles and 45° AOI. The yellow curves show the envelopes of the as-pulse trains containing harmonics 8–10 in the respective simulations.

these are the dominant harmonics transmitted through the In filter in our experiment containing close to 90% of the total XUV energy. In this case, the durations of the as-pulses are 500 as for $L = 0.05\lambda_L$ and 850 as for $L = 0.2\lambda_L$.

Owing to the similarity of the spectra used in the simulation and the model calculation, one can compare the results of both approaches to assess the validity of our simple model. For $L = 0.05\lambda_L$ both the model and the simulation give very similar values for the pulse duration close to the Fourier-limited one. While for longer scale lengths the simulation does not reproduce the dip in pulse duration predicted by the model at $L = 0.2\lambda_L$, the value of 850 as is in very good agreement with the modeled pulse duration in the range of scale lengths between $0.1\lambda_L$ and $0.3\lambda_L$ (see figure 9(b)). All in all, a comparison between the analytical model and the simulations demonstrates that the model calculation, despite its simplicity, is quite capable of predicting the effect of a density gradient on the duration of the emitted as-pulses.

It is again interesting to see that the simulations with a density gradient deliver pulse durations much closer to the measured ones than those without a gradient. While, as discussed above, this cannot be seen as a proof that the harmonics are generated in a gradient owing to the large error in the measurement, it provides further evidence of such an effect and motivates the development of more complete characterization methods for as-pulses generated from solid targets.

6. Advanced characterization schemes for shorter as-pulses

The main limitation of the applied approach in this paper is the requirement for a pure two-photon ionization of helium, which restricts the spectral bandwidth of the as-pulse to be characterized only to those harmonics that do not allow single-photon ionization. In addition,

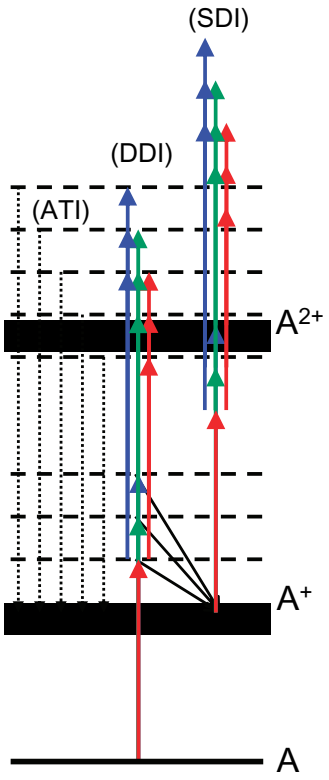

Figure 11. Schematic diagram showing the ATI, DDI and SDI processes of an atom A. While ATI leads to the generation of a singly charged ion and PEs with energies depending on the energies of the photons involved in the ionization process DDI and SDI generate doubly charged ions and PEs allowing an extension of the AC method presented in this paper to higher photon energies.

the method does not provide any phase information. In the following, we show how the XUV AC of surface harmonics can be extended to shorter wavelengths and improved to allow the retrieval of the phase between the individual harmonics.

6.1. Alternate two-XUV-photon processes for higher-order harmonic compositions

As discussed above, the ionization threshold of He ($IP_{\mathrm{He}} = 24.59\,\mathrm{eV}$) sets an upper limit to the harmonic order q that is permitted to be included in the superposition and thus a lower limit to the duration of the characterized XUV pulse. In order to overcome this limitation, an alternative two-XUV-photon ionization scheme has to be used. Possible schemes are the non-resonant direct double ionization (DDI), sequential double ionization (SDI) or ionic ionization (II) and above threshold ionization (ATI) (see figure 11) [34, 35, 48]. In these schemes, ionic products such as electrons or ions are to be detected utilizing energy resolved PE or TOF ion-mass spectroscopy, respectively.

The ATI scheme allows the continuous extension of the second-order AC method to shorter wavelengths. Provided that the region of the continuum reached by the ATI process is structureless (no autoionizing bound states are embedded in the continuum), the only restriction of the method is the rapidly decreasing cross-section with photon energy ($\propto (\hbar\omega)^{-6}$ [49]).

The two-photon-ATI scheme leads to the production of A^+ ions and electrons with energies $PE_{ch}^{ATI} = \hbar\omega_{ch} - IP_1$, where $ch = q_{min} + q_{max} + n$ with $n = 1 - N \ldots N - 1$, q_{min} and q_{max} the minimum and maximum harmonic orders, N the number of harmonics in the superposition and IP_1 the first ionization potential of the atom. The method requires energy-resolved PE spectroscopy.

The DDI and SDI schemes allow the extension of the second-order AC method to shorter wavelengths with photon energies in the region $IP_1 < \hbar\omega_q < IP_2 - IP_1$, where IP_2 in analogy to IP_1 is the second ionization potential of the atom. Here, ion mass spectrometry, selecting the doubly charged ions, or PE spectroscopy can be used. For this photon energy region, ionization processes such as single-photon, two-photon DDI (TPDDI) and three-photon SDI (ThPSDI) can contribute, with different rates, to the ionic products. In the present discussion, the single-photon ionization mechanism has been ignored since it does not contain any information about the temporal pulse characteristics. The TPDDI and ThPSDI schemes lead to the production of doubly charged ions (A^{2+}) and electrons with energies $0 < PE_{ch}^{DDI} < \hbar\omega_{ch} - IP_2$ and $PE_{ch}^{ThPSDI} = \hbar\omega_{ch} - (IP_2 - IP_1)$, respectively. Since both schemes coexist in the ionization process, the temporal evolution of the system can be evaluated at different intensities using rate equations [50, 51]. Nevertheless, according to previous studies [34, 35, 48, 50, 51] in He, Ar and Kr, the intensity regions where DDI or SDI could be used for as-pulse-train characterization by means of second-order AC can be roughly estimated. Based on previous studies in He [51], for $I_{XUV} < 10^{13}\,W\,cm^{-2}$, far below the SDI saturation intensities, the TPDDI and ThPSDI rates can be expressed as

$$W_2^{DDI} = \sigma_{DDI}^{(2)} \frac{I_{XUV}^{(q)} I_{XUV}^{(p)}}{\hbar^2 \omega_q \omega_p} \quad \text{and} \quad W_3^{ThPSDI} = \sigma^{(1)} \frac{I_{XUV}^{(q)}}{\hbar\omega_q} \sigma_{TPII}^{(2)} \frac{I_{XUV}^{(q)} I_{XUV}^{(p)}}{\hbar^2 \omega_q \omega_p}, \tag{5}$$

respectively. Here σ_{TPII} denotes the two-photon ionization cross-section of the ion. DDI is then the dominant process that could be used for as-pulse characterization. For much higher intensities ($I_{XUV} > 3 \times 10^{15}\,W\,cm^{-2}$), far above the SPI saturation intensities, the ThPSDI rate may by written as the product of the ionic saturated ground state population times the ionic two-photon ionization rate, i.e.

$$W_3^{ThPSDI} = \frac{Y_1^{(q)}}{N} \sigma_{TPII}^{(2)} \frac{I_{XUV}^{(q)} I_{XUV}^{(p)}}{\hbar^2 \omega_q \omega_p}, \tag{6}$$

which indicates a second-order process. In this case, the SDI process is the dominant one that could be used for a measurement of the as-pulse duration.

A list of the possible candidate rare gas atoms that could be used for the characterization process using the DDI or SDI schemes and their properties are shown in table 1. The fifth and sixth columns depict the photon energy window and the corresponding maximum and minimum harmonic orders (assuming that the wavelength of the fundamental is 800 nm), which could be used in implementing the DDI and SDI schemes. The seventh column shows the minimum harmonic order required for TPDI.

6.2. Toward XUV-FROG–type measurements

So far, the direct measurement of the spatiotemporally averaged duration of the individual pulses of an as-pulse train was based on the second-order AC technique [24, 32]. An extension of the technique to a frequency-resolved optical gating (FROG)-like approach will

Table 1. Possible candidate rare gas atoms, photon energies and harmonic orders (assuming that the wavelength of the fundamental is 800 nm) that could be used for the characterization of as-pulse trains by means of second-order AC technique using DDI or SDI schemes.

Atom	IP_1 (eV)	IP_2 (eV)	IP_2-IP_1 (eV)	$\hbar\omega_{q_{min}}, \hbar\omega_{q_{max}}$ (eV)	q_{min}, q_{max}	$q_{min\,2-ph.}$
He	24.59	79.01	54.42	24.59, 54.42	16, 35	26
Ne	21.56	65.72	44.16	21.56, 44.16	14, 28	22
Ar	15.76	43.39	27.63	15.76, 27.63	11, 17	14
Kr	14.00	38.36	24.36	14.00, 24.36	9, 15	13
Xe	12.13	33.13	21.00	12.13, 21.00	8, 13	11

provide detailed information, i.e. spectral phase distributions, allowing the reconstruction of the temporal profile of the as-pulses in the train. This approach requires measurement of frequency-resolved two-XUV-photon ionization traces, which can be recorded applying energy-resolved PE spectroscopy. While second-order AC-based FROG-type measurements of individual harmonics [52, 53] and mode-resolved AC measurements of an as-pulse train generated in a gas-phase medium have been demonstrated [32], FROG-type measurements of attosecond trains have not yet been successfully demonstrated. In well-established femtosecond metrology, the FROG trace corresponds to the mapping of the phase-amplitude distribution of the pulse to be characterized [54]. A FROG trace in the second-order geometry is given by

$$I_{\mathrm{FROG}}^{\mathrm{SHG}}(\tau,\omega) = \left| \int_{-\infty}^{\infty} E(t)E(t-\tau)\exp(-\imath\omega t)\,\mathrm{d}t \right|^2, \tag{7}$$

where $E(t)$ is the electric field of the pulse to be characterized and τ is the delay introduced between the two pulse replicas. The $I_{\mathrm{FROG}}^{\mathrm{SHG}}$ corresponds to the spectrogram recorded in the spectral region of the second harmonic generated in the interaction of the superposition of the two parts of the pulse in a nonlinear crystal. For the characterization of the pulse, a FROG algorithm has to be used [54].

For as-pulse trains a second-order FROG trace becomes more complex owing to the fact that a whole series of harmonics of the fundamental frequency are present in the interaction volume. In an XUV-wavefront splitting geometry, the FROG trace is given by

$$I_{\mathrm{FROG}}^{\mathrm{XUV}}(\tau,\omega) \propto \left| \sum_{p,q}^{N} \int_{-\infty}^{\infty} E_p(t)E_q(t-\tau)\exp(-\imath\omega t)\,\mathrm{d}t \right|^2, \tag{8}$$

where p and q correspond to the harmonic order, N is the maximum harmonic order used in the superposition, $E_{p,q}$ are the harmonic electric fields and τ is the delay between the two replicas of the XUV pulse train. In this case, $I_{\mathrm{FROG}}^{\mathrm{XUV}}$ is a spectrogram recorded by measuring the two-XUV-photon ionization PE signal. The excess energy of each ionization channel, i.e. each electron peak energy, is given by $E_{\mathrm{ch}} = \hbar(\omega_p + \omega_q) - IP_{\mathrm{He}}$.

For the harmonics generated via the CWE mechanism, where different harmonics originate from different depths inside the target [12, 43], the phase relation between the individual harmonics would map out the density gradient on the plasma surface, thus providing additional information about the pre-plasma evolution with femtosecond resolution. In order to illustrate

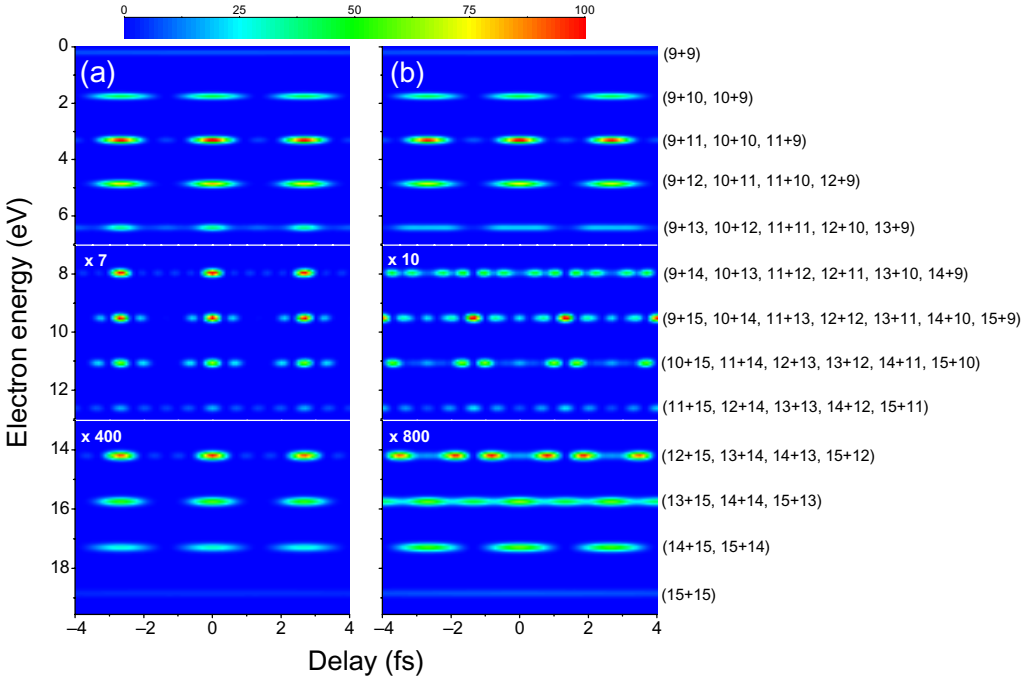

Figure 12. Calculated XUV-FROG trace of an as-pulse train. Harmonics H8–H14 are used in the superposition with relative field amplitudes 0.83 (H8) : 1 (H9) : 1 (H10) : 0.2 (H11) : 0.16 (H12) : 0.24 (H13) : 0.18 (H14) corresponding to the relative transmission values of an In filter like the one used in our experiment. The traces are calculated for (a) zero relative phase between the harmonics and (b) a relative phase between the harmonics of $\Delta\phi_q = (q - q_{\min})^3$ (with $q_{\min} = 8$). In both cases, the harmonic chirp is assumed to be zero.

the effect of the phase introduced into the XUV-FROG trace by the CWE harmonics generated at a linear density gradient, figure 12 shows the calculated XUV-FROG trace of an as-pulse train, in the range of −4 fs to +4 fs delay for (a) zero relative phase between the harmonics and (b) a relative phase of $\Delta\phi_q = (q - q_{\min})^3$ (with $q_{\min} = 8$) corresponding to the phase introduced by a linear density gradient in the CWE mechanism (see section 5.1 and [43]). In both cases the chirp within the harmonic bandwidth is assumed to be zero. In the calculation, the harmonics H8–H14 are used in the superposition with relative field amplitudes 0.83 (H8) : 1 (H9) : 1 (H10) : 0.2 (H11) : 0.16 (H12) : 0.24 (H13) : 0.18 (H14) corresponding to the relative transmission values of an In filter like the one used in our experiment. This shows that with the experimental setup presented in this paper, it should, in principle, also be possible to measure the phase between the individual harmonics by replacing the ion TOF by a PE spectrometer. However, this is in practice not a trivial issue, as an ultrahigh resolution PE spectrometer [55] is necessary and the electron signal is much weaker than the one obtained from ion TOF. Nevertheless, improvements in the transport of the generated harmonics to the interaction region should make high enough XUV intensities possible in the not-so-distant future [36], making the method described above feasible.

7. Conclusions

In conclusion, we have given a detailed account of the first experiment directly studying the temporal characteristics of high harmonics emitted from solid-density targets using XUV AC. Our experiments have demonstrated for the first time that the harmonic emission from solid targets in the CWE regime is indeed phase locked and emitted as a train of sub-femtosecond (approximately 900 as) pulses with an overall duration similar to the one of the driving laser and thus possesses the most important property necessary for a next-generation as-pulse source of unprecedented brightness.

In addition to the presentation of the AC results, we have given a detailed account of the setup and functionality of the volume-AC setup used and analyzed its functionality under realistic conditions. Based on the current understanding of the CWE harmonic generation mechanism, we have developed a simple model to assess the influence of a pre-plasma gradient on the duration of the individual as-pulses and demonstrate that the pulse duration measured could indeed be explained by a pre-expansion of the solid-density target of the order of $0.1–0.3\lambda_L$. While the error of the AC measurement is too large to positively confirm this, such a gradient would be in good agreement with pre-ionization owing to the limited picosecond contrast of the ATLAS laser system used for the experiment.

Inspired by the demonstration that the harmonic emission is indeed phase locked, we present several possible methods to expand our temporal characterization for solid harmonics to higher photon energies and we suggest an approach to reconstruct the relative phase between the individual harmonics.

All in all, our findings open the path toward further development of surface-harmonics-based as-sources for applications and promise to make possible a whole new category of XUV-pump–XUV-probe-type experiments investigating nonlinear processes not accessible with current moderate energy as-pulse sources based on harmonic generation in noble gases.

Acknowledgments

This work was partially supported by the DFG-project TR18, by the Munich Center for Advanced Photonics (MAP), by the European Community's Human Potential Programme under contract number MRTN-CT-2003-505138 (XTRA), by the FP6 project 'Laserlab-Europe', contract number RII3-CT-2003-506350 and by the Association EURATOM–Max-Planck-Institut für Plasmaphysik. SGR acknowledges financial support from the International Max Planck Research School on Advanced Photon Science (IMPRS-APS).

References

[1] Paul P M, Toma E S, Breger P, Mullot G, Auge F, Balcou Ph, Muller H G and Agostini P 2001 Observation of a train of attosecond pulses from high harmonic generation *Science* **292** 1689–92
[2] Hentschel M, Kienberger R, Spielmann Ch, Reider G A, Milosevic N, Brabec T, Corkum P, Heinzmann U, Drescher M and Krausz F 2001 Attosecond metrology *Nature* **414** 509–13
[3] Goulielmakis E *et al* 2004 Direct measurement of light waves *Science* **305** 1267–9
[4] Uiberacker M *et al* 2007 Attosecond real-time observation of electron tunnelling in atoms *Nature* **446** 627–32
[5] Cavalieri A L *et al* 2007 Attosecond spectroscopy in condensed matter *Nature* **449** 1029–32

[6] Rundquist A, Durfee C G III, Chang Z, Herne C, Backus S, Murnane M M and Kapteyn H C 1998 Phase-matched generation of coherent soft x-rays *Science* **280** 1412–5
[7] Tamaki Y, Itatani J, Nagata Y, Obara M and Midorikawa K 1999 Highly efficient, phase-matched high-harmonic generation by a self-guided laser beam *Phys. Rev. Lett.* **82** 1422–5
[8] Constant E, Garzella D, Breger P, Mével E, Dorrer Ch, Le Blanc C, Salin F and Agostini P 1999 Optimizing high harmonic generation in absorbing gases: model and experiment *Phys. Rev. Lett.* **82** 1668–71
[9] Krausz F and Ivanov M 2009 *Attosecond Phys. Rev. Mod. Phys.* **81** 163–234
[10] Tsakiris G D, Eidmann K, Meyer-ter Vehn J and Krausz F 2006 Route to intense single attosecond pulses *New J. Phys.* **8** 19
[11] Baeva T, Gordienko S and Pukhov A 2006 Theory of high-order harmonic generation in relativistic laser interaction with overdense plasma *Phys. Rev.* E **74** 046404
[12] Quéré F, Thaury C, Monot P, Dobosz S, Martin P, Geindre J-P and Audebert P 2006 Coherent wake emission of high-order harmonics from overdense plasmas *Phys. Rev. Lett.* **96** 125004
[13] Tarasevitch A, Lobov K, Wuensche C and von der Linde D 2007 Transition to the relativistic regime in high order harmonic generation *Phys. Rev. Lett.* **98** 103902
[14] Lichters R and Meyer-ter Vehn J 1997 *Multiphoton Processes (Inst. Phys. Conf. Ser. No. 154)* pp 221–30
[15] Bulanov S V, Naumova N M and Pegoraro F 1994 Interaction of an ultrashort, relativistically strong laser pulse with an overdense plasma *Phys. Plasmas* **1** 745–57
[16] Gordienko S, Pukhov A, Shorokhov O and Baeva T 2004 Relativistic Doppler effect: universal spectra and zeptosecond pulses *Phys. Rev. Lett.* **93** 115002
[17] Brunel F 1987 Not-so-resonant, resonant absorption *Phys. Rev. Lett.* **59** 52
[18] Thaury C *et al* 2007 Plasma mirrors for ultrahigh-intensity optics *Nat. Phys.* **3** 424–9
[19] Dromey B 2007 Bright multi-keV harmonic generation from relativistically oscillating plasma surfaces *Phys. Rev. Lett.* **99** 085001
[20] Dromey B *et al* 2009 Diffraction limited performance and focusing of high harmonics from relativistic plasmas *Nat. Phys.* **5** 146–52
[21] Hörlein R *et al* 2008 High contrast plasma mirror: spatial filtering and second harmonic generation at 10^{19} W cm^{-2} *New J. Phys.* **10** 083002
[22] Thaury C, George H, Quéré F, Loch R, Geindre J-P, Monot P and Martin Ph 2008 Coherent dynamics of plasma mirrors *Nat. Phys.* **4** 631–4
[23] Dromey B *et al* 2006 High harmonic generation in the relativistic limit *Nat. Phys.* **2** 456–9
[24] Nomura Y *et al* 2009 Attosecond phase-locking of harmonics emitted from laser-produced plasmas *Nat. Phys.* **5** 124–8
[25] Iaconis C and Walmsley I A 1998 Spectral phase interferometry for direct electric-field reconstruction of ultrashort optical pulses *Opt. Lett.* **23** 792–4
[26] Cormier E, Walmsley I A, Kosik E M, Wyatt A S, Corner L and DiMauro L F 2005 Self-referencing, spectrally, or spatially encoded spectral interferometry for the complete characterization of attosecond electromagnetic pulses *Phys. Rev. Lett.* **94** 033905
[27] Itatani J, Quéré F, Yudin G L, Ivanov Yu M, Krausz F and Corkum P B 2002 Attosecond streak camera *Phys. Rev. Lett.* **88** 173903
[28] Kienberger R *et al* 2002 Steering attosecond electron wave packets with light *Science* **297** 1144–8
[29] Kobayashi Y, Sekikawa T, Nabekawa Y and Watanabe S 1998 27-fs extreme ultraviolet pulse generation by high-order harmonics *Opt. Lett.* **23** 64–6
[30] Tzallas P, Charalambidis D, Papadogiannis N A, Witte K and Tsakiris G D 2003 Direct observation of attosecond light bunching *Nature* **426** 267–70
[31] Sekikawa T, Kosuge A, Kanai T and Watanabe S 2004 Nonlinear optics in the extreme ultraviolet *Nature* **432** 605–8
[32] Nabekawa Y, Shimizu T, Okino T, Furusawa K, Hasegawa H, Yamanouchi K and Midorikawa K 2006 Conclusive evidence of an attosecond pulse train observed with the mode-resolved autocorrelation technique *Phys. Rev. Lett.* **96** 083901

[33] Furusawa K, Okino T, Shimizu T, Hasegawa H, Nabekawa Y, Yamanouchi K and Midorikawa K 2006 Photoelectron spectroscopy of two-photon ionisation of rare-gas atoms by multiple high order harmonics *Appl. Phys.* B **83** 203–11

[34] Nabekawa Y, Hasegawa H, Takahashi E J and Midorikawa K 2005 Production of doubly charged helium ions by two-photon absorption of an intense sub-10-fs soft x-ray pulse at 42 eV photon energy *Phys. Rev. Lett.* **94** 043001

[35] Benis E P, Charalambidis D, Kitsopoulos T N, Tsakiris G D and Tzallas P 2006 Two-photon double ionization of rare gases by a superposition of harmonics *Phys. Rev.* A **74** 051402

[36] Hörlein R, Nomura Y, Osterhoff J, Major Zs, Karsch S, Krausz F and Tsakiris G D 2008 High harmonics from solid surfaces as a source of ultra-bright XUV radiation for experiments *Plasma Phys. Control. Fusion* **50** 124002

[37] Tzallas P, Charalambidis D, Papadogiannis N A, Witte K and Tsakiris G D 2005 Second-order autocorrelation measurements of attosecond XUV pulse trains *J. Mod. Opt.* **53** 321–40

[38] Lidle D R (ed) 2004 *CRC Handbook of Chemistry and Physics* 85th edn (Boca Raton, FL: CRC Press)

[39] Marr G V and Best J B 1976 Absolute photoionization cross-section tables for helium, neon, argon, and krypton in the VUV spectral regions *At. Data Nucl. Data Tables* **18** 497

[40] Saenz A and Lambropoulos P 1999 Theoretical two-, three- and four-photon ionization cross sections of helium in the XUV range *J. Phys. B: At. Mol. Opt. Phys.* **32** 5629–37

[41] Nomura Y 2008 Temporal characterization of harmonic radiation generated by intense laser–plasma interaction *PhD Thesis* Ludwig-Maximilians, Universität München

[42] Mashiko H, Suda A and Midorikawa K 2003 All-reflective interferometric autocorrelator for the measurement of ultra-short optical pulses *Appl. Phys.* B **76** 525–30

[43] Hörlein R, Nomura Y, Rykovanov S, Krausz F and Tsakiris G D 2009 Factors influencing the temporal characteristics of coherent wake field harmonic emission from solid surfaces *Proc. SPIE* **7359** 73590D

[44] Goupillaud P, Grossmann A and Morlet J 1984 Cycle-octave and related transforms in seismic signal analysis *Geoexploration* **23** 85–102

[45] Rykovanov S, Geissler M, Meyer-ter Vehn J and Tsakiris G D 2008 Intense single attosecond pulses from surface harmonics using the polarization gating technique *New J. Phys.* **10** 025025

[46] Quéré F, Thaury C, Geindre J-P, Bonnaud G, Monot P and Martin Ph 2008 Phase properties of laser high-order harmonics generated on plasma mirrors *Phys. Rev. Lett.* **100** 095004

[47] Dromey B *et al* 2009 Tuneable enhancement of high harmonic emission from laser–solid interactions *Phys. Rev. Lett.* **102** 225002

[48] Miyamoto N, Kamei M, Yoshitomi D, Kanai T, Sekikawa T, Nakajima T and Watanabe S 2004 Observation of two-photon above-threshold ionization of rare gases by XUV harmonic photons *Phys. Rev. Lett.* **93** 083903

[49] Faisal F H M 1987 *Theory of Multiphoton Processes* (New York: Plenum)

[50] Kornberg N A and Lambropoulos B 1999 Photoelectron energy spectrum in direct two-photon double ionization of helium *J. Phys. B: At. Mol. Opt. Phys.* **32** L603–13

[51] Lambropoulos P, Nikolopoulos L A A and Makris M G 2005 Signatures of direct double ionization under XUV radiation *Phys. Rev.* A **72** 013410

[52] Kosuge A, Sekikawa T, Zhou X, Kansai T, Adachi S and Watanabe S 2006 Frequency-resolved optical gating of isolated attosecond pulses in the extreme ultraviolet *Phys. Rev. Lett.* **97** 263901

[53] Sekikawa T, Katsura T, Miura S and Watanabe S 2002 Measurement of the intensity-dependent atomic dipole phase of a high harmonic by frequency-resolved optical gating *Phys. Rev. Lett.* **88** 193902

[54] Trebino R, DeLong K W, Fittinghoff D N, Sweetser J N, Krumbügel M A, Richman B A and Kane D J 1997 Measuring ultrashort laser pulses in the time–frequency domain using frequency-resolved optical gating *Rev. Sci. Instrum.* **68** 3277–95

[55] Kruit P and Read F H 1983 Magnetic field paralleliser for 2π; electron-spectrometer and electron-image magnifier *J. Phys. E: Sci. Instrum.* **16** 313–24